arXiv:1001.2074v1 [hep-ph] 13 Jan 2010

AS-TEXONO/10-02
January 13, 2010

Enhanced Sensitivities for the Searches of Neutrino Magnetic Moments through Atomic Ionization

Henry T. Wong[1], Hau-Bin Li, and Shin-Ted Lin

Institute of Physics, Academia Sinica, Taipei 115, Taiwan.

Abstract

A new detection channel on atomic ionization for possible neutrino electromagnetic interactions was identified and studied. Significant enhancement can be expected when the energy transfer to the target is of the atomic-transition scale. Interaction cross-section induced by neutrino magnetic moments (μ_ν) was evaluated with the equivalent photon method. New limit of $\mu_\nu(\bar{\nu_e}) < 1.3\times10^{-11}$ μ_B at 90% confidence level was derived using current data with reactor neutrinos. Potential reaches of future experiments were explored. Experiments with sub-keV sensitivities can probe μ_ν to $\sim 10^{-13}$ μ_B. Positive observations of μ_ν in this range would imply that neutrinos are Majorana particles.

PACS Numbers: 14.60.Lm, 13.15.+g, 13.40.Em

[1]Corresponding Author – htwong@phys.sinica.edu.tw; Tel:+886-2-2789-6789; FAX:+886-2-2788-9828.

The compelling evidence of neutrino oscillations implies finite neutrino masses and mixings [1]. The origins and implications remain to be fully explored and understood. Experimental studies on neutrino properties and interactions can shed light to these fundamental questions and provide constraints to models on new physics.

The possible couplings of neutrinos with the photons [2, 3, 4] are important intrinsic properties and generic consequences of finite neutrino masses. The neutrino electromagnetic vertex can be formulated as

$$\Gamma^{\mu} \;=\; \frac{1}{6}\, q^2 \,\langle r_{\nu}^2 \rangle \,\gamma^{\mu} \;+\; \frac{\mu_{\nu}}{2m_e}\,\sigma^{\mu\nu}\, q_{\nu} \qquad (1)$$

where m_e is the electron mass and $q{=}(\nu;\vec{q})$ is the four-momentum of the virtual photon γ^*. The parameters $\langle r_{\nu}^2 \rangle$ and μ_{ν} (in units of the Bohr magneton $\mu_{\rm B}$) are the "neutrino charge radius" and "neutrino magnetic moment", respectively, and describe interactions without and with helicity change. We report an interaction channel which significantly enhances the detection sensitivities of neutrino-photon couplings and place limits on $\mu_{\nu}(\bar{\nu_{\rm e}})$ with reactor neutrino data. There are controversial interpretations on whether $\langle r_{\nu}^2 \rangle$ is a physical observable [3]. The contributions of this channel to $\langle r_{\nu}^2 \rangle$ will be the subject of subsequent investigations.

The parameter μ_{ν} is an effective parameter depending on the eigenstate compositions at the detectors [4]. The study of μ_{ν} is, in principle, a way to distinguish between Dirac and Majorana neutrinos [2] $-$ a crucial unresolved issue in neutrino physics. The most sensitive laboratory measurements on μ_{ν} [5] are from neutrino-electron scattering experiments with reactor [6, 7] and solar neutrinos [8], where the most stringent published limits are $\mu_{\nu}(\bar{\nu_{\rm e}}) < 7.4 \times 10^{-11}\ \mu_{\rm B}$ [6] and $\mu_{\nu}(\nu_{\odot}) < 5.4 \times 10^{-11}\ \mu_{\rm B}$ [8], at 90% confidence level (CL), respectively. For exactness, the "electron" in this context should be specified to be free electron (FE). The differential cross-section is given by [4]

$$(\frac{d\sigma}{dT})^{FE} \;=\; \frac{\pi\alpha_{em}^2 {\mu_{\nu}}^2}{m_e^2}[\frac{1-T/E_{\nu}}{T}]\ , \qquad (2)$$

where $\alpha_{em} = e^2/4\pi$ is the fine-structure constant, m_e the electron mass, E_{ν} the neutrino energy and T the experimentally observable electron recoil energy. This expression is valid when T is much larger than the atomic scale (typically <10 keV). Otherwise, the target is no longer FE and the atomic binding energy (Δ_b) will lead to suppression in $(d\sigma/dT)^{FE}$ and in the analogous Standard Model (SM) ν-e cross-section [9].

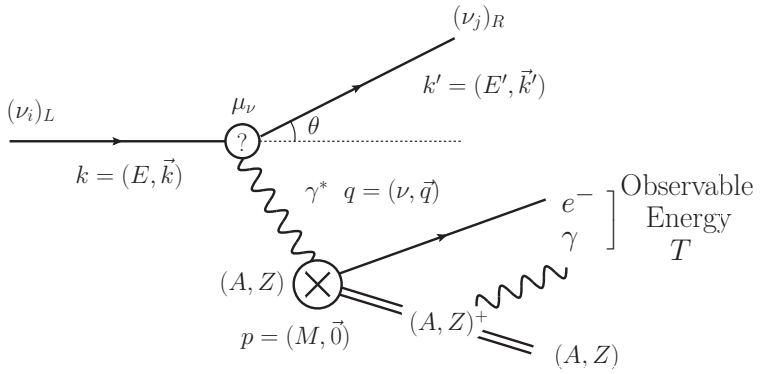

Figure 1: Schematics of the neutrino magnetic moment interaction via the atomic ionization channel. The kinematical variables for the incoming and outgoing particles are defined in the target rest frame, following standard notations.

When the energy transfer is comparable to the atomic scale, a new channel corresponding to atomic ionization (AI) becomes available:

$$\begin{aligned} \nu \ + \ (A,Z) \quad &\rightarrow \quad \nu \ + \ (A,Z)^+ \ + \ e^- \\ (A,Z)^+ \quad &\rightarrow \quad (A,Z) \ + \gamma \ 's \quad . \end{aligned} \tag{3}$$

This is a t-channel process, depicted schematically in Figure 1. The target atom (A, Z) is probed and ionized electromagnetically, resembling the photoelectric effect induced by γ^* instead of physical photons. Experimental observables are the kinetic energy of the ejected electron and the absorption of the subsequent X-rays, the sum of which is $T{=}E_\nu - E'_\nu$. As $T \sim \Delta_b$, the $q^2 \rightarrow 0$ parameter space becomes kinematically allowed [10]. The AI cross-section is therefore enhanced relative to that of FE, where $q^2{=}{-}2\ m_e\ T$. Atomic enhancement in absorption cross-sections has been studied for "weakly interacting absorbable particles" like axions [11]. Resonant orbital electron capture induced by $\bar{\nu_e}$ has been considered for the detection of low energy geo-neutrinos [12].

The neutrino electromagnetic AI processes are analogous to the SM electromagnetic interactions (QED) of relativistic charged particles on matter which were well-studied experimentally and theoretically [10, 13]. The average macroscopic energy loss is described by the "dE/dx"-formula which is the cornerstone of detector system design. Several channels are involved at the interaction-by-interaction level. The AI process dominates at atomic-scale energy as $T \sim \Delta_b$, as characterized by

the distinct peak structures in Figure 6 of Ref. [10]. This is the basis of relativistic charged probes being "minimum ionizing". Rutherford scatterings of FE produce a smooth continuum several orders of magnitude weaker. Small contributions from Cerenkov radiations can be neglected. The QED AI process can be denoted by Figure 1 − except that the μ_ν coupling is replaced by the standard QED vertex described by the lepton current

$$l^\mu(e) \;=\; \bar{u}_j(k')\;\gamma^\mu\;u_i(k)\;. \tag{4}$$

The AI enhancement will not occur in SM t-channel ν-e scatterings [9], or in astrophysics media with temperature high enough to be in plasma states.

Following the case for QED [10, 14], the equivalent photon approximation (EPA) method [15] was used to evaluate the μ_ν-induced AI cross-section of Figure 1. The measurable $(d\sigma/dT)^{AI}$ is expressed in terms of absorption cross-section for physical photons. This is justified since $q^2 \to 0$ at $T \sim \Delta_b$, such that γ^* can be taken as nearly real. The EPA approach was adopted in a similar work studying μ_ν-induced photo-disintegration of deuterium [16]. The cross-section was derived following the standard formalism developed for inelastic lepton-hadron scattering described stepwise in, for instance, Ref. [17]. The kinematical variables of the neutrino probe and atomic target are defined in the target rest frame using the standard notations shown in Figure 1. The energy component of γ^* is $\nu \equiv E_\nu - E'_\nu = T$. The QED lepton current of Eq. 4 is replaced by the μ_ν current:

$$l^\mu(\mu_\nu) \;=\; \frac{\mu_{ij}}{2m_e}\;\bar{u}_j(k')\;\sigma^{\mu\nu}\;u_i(k)\;q_\nu \tag{5}$$

where μ_{ij} is the coupling between neutrino mass eigenstates $\nu_{\rm i}$ and $\nu_{\rm j}$ with the photon. Symmetry principles constrain that $i \neq j$ for Majorana neutrinos [2]. The cross-section can be expressed as [17]

$$\frac{d\sigma}{dE'_\nu\;d\Omega} = \frac{E'_\nu}{E_\nu}\frac{\alpha^2_{em}}{(q^2)^2}\;L^{\mu\nu}\;W_{\mu\nu} \tag{6}$$

where $L^{\mu\nu}$ is the neutrino current tensor which, after summations over $\nu_{i,j}$, is given by [16]

$$\begin{aligned} L^{\mu\nu} \;&\equiv\; <[l^\mu(\mu_\nu)]^\dagger[l^\nu(\mu_\nu)]> \\ &=\; \frac{\mu^2_\nu}{4m^2_e}\;q^2\;[q^\mu q^\nu + 2(k'^\mu k^\nu + k'^\nu k^\mu)] \end{aligned} \tag{7}$$

and $W_{\mu\nu}$ parameterizes the target current tensor.

The target tensor for μ_ν-induced FE scattering is simply given by the spin-averaged QED lepton current of Eq. 4 scaled by appropriate phase-space and normalization factors. The FE cross-section of Eq. 2 can be reproduced following Eq. 6. The target tensor for the AI channel can be parameterized with two structure functions $F_a(q^2,\nu)$ and $F_b(q^2,\nu)$ [16]:

$$\begin{aligned} W^{AI}_{\mu\nu} &= F_a\ [-\frac{q^2}{p\cdot q}p_\mu p_\nu - (p\cdot q)g_{\mu\nu} + p_\mu q_\nu + p_\nu q_\mu] \\ &\quad + F_b\ [q^2 g_{\mu\nu} - q_\mu q_\nu]\ . \end{aligned} \tag{8}$$

Accordingly, Eq. 6 becomes

$$\begin{aligned} (\frac{d\sigma}{dE'_\nu\ d\Omega})^{AI} &= \frac{E'_\nu}{E_\nu}\ \frac{\alpha^2_{em}}{(q^2)^2}\ \frac{\mu^2_\nu}{4m^2_e} \\ &\quad 4\ (q^2)^2\ \frac{(p\cdot k)^2}{(p\cdot q)}\ \left[F_a(-1+\frac{p\cdot q}{p\cdot k}) - F_b\frac{1}{4}\frac{p\cdot q}{(p\cdot k)^2}q^2\right]\ . \end{aligned} \tag{9}$$

As $q^2\to 0$, the total virtual photon cross-section ($\sum_\lambda \sigma_{\gamma^*_\lambda}$) is dominated by contributions from the two transverse components ($\lambda=\pm$). The photoelectric cross-section of physical photons ($\sigma_{\gamma A}$) [18] is therefore given by [16, 17]

$$\begin{aligned} 2\ \sigma_{\gamma A} = (\sigma_{\gamma^*_+} + \sigma_{\gamma^*_-}) \ &\rightarrow\ \sum_\lambda\ \sigma_{\gamma^*_\lambda} = \frac{4\pi^2\alpha_{em}}{\nu}(-g^{\mu\nu}\ W^{AI}_{\mu\nu}) \\ \text{so that} \qquad \sigma_{\gamma A} &\simeq \frac{1}{2}\ [\frac{4\pi^2\alpha_{em}}{\nu}\ 2\ (p\cdot q)\ F_a]\ . \end{aligned} \tag{10}$$

Combining Eqs. 9&10, substituting $(p\cdot q)=M\nu$, $(p\cdot k)=ME_\nu$ in the laboratory frame where M is the target mass, and taking leading term using $(\nu = T) \ll E_\nu$ and $F_b q^2 \to 0$, the μ_ν-induced AI cross-section is:

$$(\frac{d\sigma}{dT})^{AI} \simeq \mu^2_\nu\ \frac{\alpha_{em}}{\pi}\ (\frac{E_\nu}{m_e})^2\ \frac{1}{T}\ \sigma_{\gamma A}(E_\gamma = T)\ . \tag{11}$$

The expression reproduces that of Ref. [16] which was checked to within 10% and 1% with alternative derivations on μ_ν-induced photo-disintegration of deuterium based on effective-range approximation and nuclear physics approach [19], respectively.

The cross-sections on Ge target due to the AI and FE channels with reactor neutrinos at $\mu_\nu = 10^{-10}\ \mu_{\rm B}$ are displayed in Figure 2, together with the SM $\bar{\nu}_{\rm e}$-e [20] and $\bar{\nu}_{\rm e}$-N coherent [21] scatterings. The realistic spectrum [6] at a typical flux of $\phi(\bar{\nu}_{\rm e})$=10^{13} cm^{-2}s^{-1} was used. The peak structures for AI are consequences of the

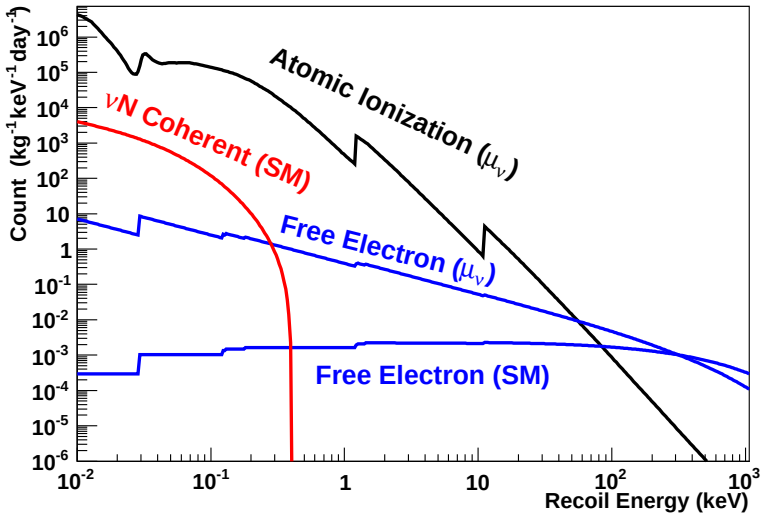

Figure 2: The observable spectra due to neutrino interactions on Ge target with reactor $\bar{\nu}_e$ at $\phi(\bar{\nu}_e)$=10^{13} cm^{-2}s^{-1}. Contributions from the AI and FE channels at μ_ν=10^{-10} μ_B, as well as from SM $\bar{\nu}_e$-e and $\bar{\nu}_e$-N coherent scattering are shown.

enhancement of $\sigma_{\gamma A}$ [18]. The AI event rates exceed those of FE by several orders of magnitude at atomic-scale energy, reproducing similar behaviour as in the QED case with charged probes [10]. The difference in lepton energy dependence (E_ν^2 versus $\sim \log[E_l]$ [10, 14] for μ_ν and QED-induced AI, respectively) originates from the differences in the current terms in Eqs. 5&4.

Limits on $\mu_\nu(\bar{\nu}_e)$ were derived with the AI channel. Two published data set with reactor neutrinos at the Kuo-Sheng Reactor Neutrino Laboratory (KSNL) at $\phi(\bar{\nu}_e) \sim 6\times10^{12}$ cm^{-2}s^{-1} were used. The first one was the Reactor ON$-$OFF residual spectrum from 570.7/127.8 days of ON/OFF data at 12 keV analysis threshold with the 1-kg high-purity germanium (HPGe) detector [6]. Alternatively, we adopted the Reactor ON spectrum with 0.338 kg-day exposure using a 20-g ultra-low-energy Ge (ULEGe) detector array at a threshold of (220$\pm$10) eV at 50% signal efficiency [22]. There was no Reactor OFF data so that the conventional Reactor ON$-$OFF background subtraction was not possible. Instead, no background assumption was made and an analysis analogous to dark matter searches was performed using standard formalism [23]. The μ_ν-induced contributions could not be larger than the observed signals and upper limit was derived. In both cases, the published statistical and systematic errors were adopted. An additional systematic effect was due to the un-

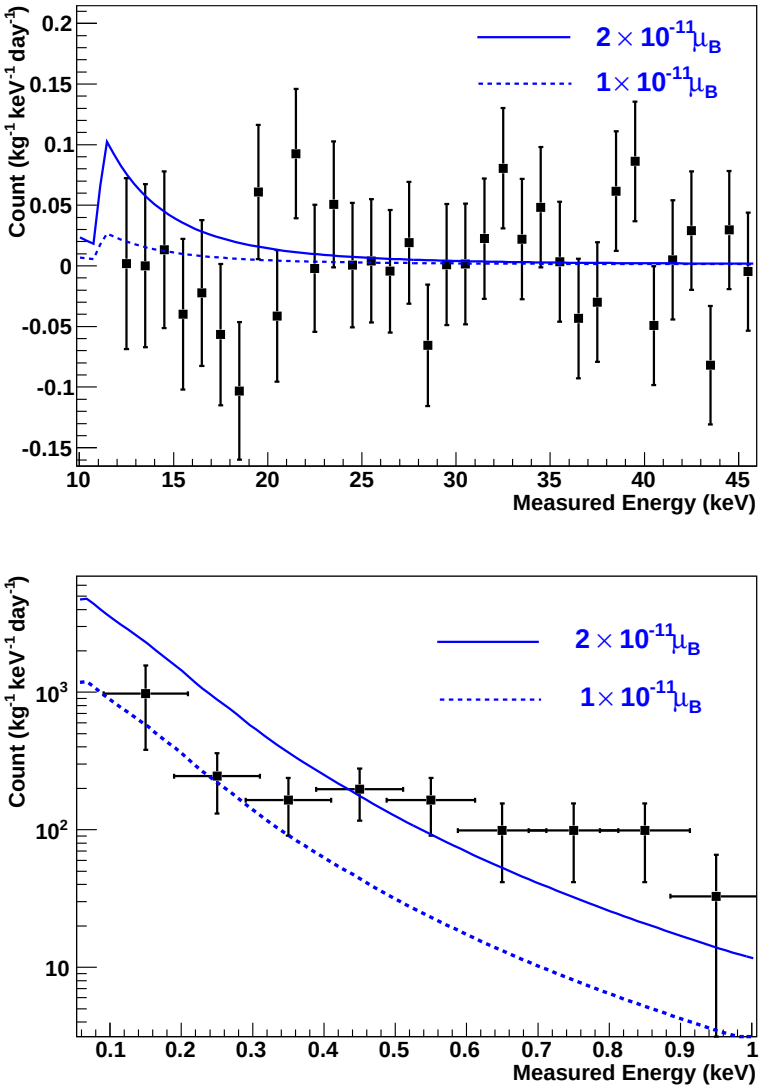

Figure 3: Top: (a) The Reactor ON−OFF residual spectrum from 1-kg HPGe at KSNL. Bottom: (b) The Reactor ON spectrum from 20-g ULEGe. The μ_ν-induced AI spectra at an allowed and an excluded values of $\mu_\nu(\bar{\nu}_e)$ are superimposed.

AmBkg (cpkkd)	Threshold (eV)	Limiting Background Mode	$\mu_\nu(\bar{\nu}_e)$ Sensitivities ($\times 10^{-12}$ μ_B) FE	AI
Current Data :				
HPGe (Ref. [6])		AmBkg	< 57	< 17
ULEGe (Ref. [22])		AmBkg	$-$	< 13
Projected Sensitivities :				
10	100	AmBkg+SM $\bar{\nu}_e$-N	30	0.3
1	100	AmBkg+SM $\bar{\nu}_e$-N	10	0.1
<0.1	100	SM ($\bar{\nu}_e$-e+$\bar{\nu}_e$-N)	4	0.04
		SM $\bar{\nu}_e$-e †	2	0.009
<0.1	10	SM ($\bar{\nu}_e$-e+$\bar{\nu}_e$-N)	4	0.04
		SM $\bar{\nu}_e$-e †	0.7	0.0009

Table 1: Limits on $\mu_\nu(\bar{\nu}_e)$ from the FE and AI channels using reactor neutrino data. The projected sensitivities assume $\phi(\bar{\nu}_e) = 10^{13}$ cm^{-2}s^{-1} and <1% uncertainty in the ON−OFF background subtraction. The superscript † denotes *ideal* experiments which can differentiate nuclear from electron recoils, so that SM $\bar{\nu}_e$-N background can be eliminated.

certainties in the EPA calculations for $(d\sigma/dT)^{AI}$. A conservative estimate of 20% was adopted for the analysis. The upper limits are summarized and compared to those of FE scattering in Table . The more stringent one is

$$\mu_\nu(\bar{\nu}_e) \ < \ 1.3 \times 10^{-11} \ \mu_B \tag{12}$$

at 90% CL with the ULEGe data. It improves over existing limits derived with the FE channel [6, 7, 8]. The HPGe residual and the ULEGe Reactor ON spectra are depicted in Figures 3a&b, respectively. The expected μ-induced AI spectra due to an allowed and an excluded values of $\mu_\nu(\bar{\nu}_e)$ (1×10^{-11} μ_B and 2×10^{-11} μ_B, respectively) are superimposed for comparison.

It is instructive to investigate the potential reach of this technique. Sensitivities are limited by ambient γ/neutron background (AmBkg) as well as by the SM $\bar{\nu}_e$-e and $\bar{\nu}_e$-N processes. The projected sensitivities on $\mu_\nu(\bar{\nu}_e)$ at $\phi(\bar{\nu}_e)$=10^{13} cm^{-2}s^{-1} under various background conditions are summarized in Table . The generic goals for current projects towards observation of $\bar{\nu}_e$-N coherent scattering at reactors

are background levels of ~ 1 kg^{-1}keV^{-1}day^{-1}(cpkkd) and detection threshold of $\sim$100 eV [21]. Assuming, in addition, that the Reactor ON$-$OFF subtraction of the ambient background is accurate to $\sim$1%, μ_ν can be probed to $\geq 10^{-13}$ $\mu_{\rm B}$. Such sensitivities exceed the astrophysics bounds [3, 5], typically at $\mu_\nu < 10^{-10} - 10^{-12}$ $\mu_{\rm B}$. In *ideal* experiments with AmBkg$<$0.1 cpkkd and capabilities of differentiating nuclear and electron recoil signatures, the sensitivities are limited by SM $\bar{\nu}_{\rm e}$-e. The potential reaches are $\geq 10^{-14}$ $\mu_{\rm B}$ and $\geq 10^{-15}$ $\mu_{\rm B}$ at 100 eV and 10 eV threshold, respectively. Similar boost in sensitivities can be expected for $\mu_\nu(\nu_\mu)$ from accelerator experiments [3], where the additional factor of E_ν^2 would compensate the reduction in neutrino flux. The AI enhancement may be relevant in the search of dark matter by resonant absorption [11] or via t-channel scattering induced by their finite electromagnetic couplings due to magnetic moment [24] or charge [25].

Minimally-Extended SM with massive Dirac neutrinos [3, 5] predicts $\mu_\nu \sim 10^{-19}[m_\nu/1\ {\rm eV}]$ $\mu_{\rm B}$ which does not produce observable consequences. Incorporation of physics such as Majorana neutrino transition moments or right-handed weak currents can significantly enhance μ_ν to the experimentally relevant ranges. Naturalness argument [26] dictates that Dirac neutrinos should have $\mu_\nu \leq 10^{-14}$ $\mu_{\rm B}$. Positive results on μ_ν-induced AI with future experiments will therefore imply that neutrinos are Majorana particles. The "smoking gun" experimental signatures are observations of peak structures at the K/L/M edges in the Reactor ON$-$OFF residual spectra, with intensity ratio $\propto [\sigma_{\gamma A}/T]$ as depicted in Figure 2. Most background processes do not generate structures in atomic transitions. Nuclear decays by electron capture do produce peaks at the K/L/M energies but at different ratios, dominated instead by captures of the K-orbitals.

The authors are grateful to J.W. Chen, H.N. Li and T.C. Yuan for consultations. This work is supported by the Academia Sinica Theme Project 2008-10, and through contract 98-9628-M-001-013 from the National Science Council, Taiwan.

References

[1] B. Kayser, Phys. Lett. **B 667**, 163 (2008), and references therein.

[2] B. Kayser, Phys. Rev. **D 26**, 1662 (1982);
J.F. Nieves, Phys. Rev. **D 26**, 3152 (1982);
R. Shrock, Nucl. Phys. **B 206**, 359 (1982).

[3] P. Vogel and A. Piepke, Phys. Lett. **B 667**, 521-523 (2008), and references therein.

[4] P. Vogel and J. Engel, Phys. Rev. **D 39**, 3378 (1989);
J.F. Beacom and P. Vogel, Phys. Rev. Lett. **83**, 5222 (1999).

[5] H.T. Wong and H.B. Li, Mod. Phys. Lett. **A 20**, 1103 (2005), and references therein.

[6] H.B. Li et al., Phys. Rev. Lett. **90**, 131802 (2003);
H.T. Wong et al., Phys. Rev. **D 75**, 012001 (2007).

[7] Z. Daraktchieva et al., Phys. Lett. **B 615**, 153 (2005);
A.G. Beda et al., arXiv:0906.1926 (2009).

[8] C. Arpesella et al., Phys. Rev. Lett. **101**, 091302 (2008).

[9] S.A. Fayans, V.Yu. Dobretsov and A.B. Dobrotsvetov, Phys. Lett. **B 291**, 1 (1992);
S.A. Fayans, L.A. Mikaelyan and V.V. Sinev, Phys. Atom. Nucl. **64**, 1475 (2001);
G.J. Gounaris, E.A. Paschos and P.I. Porfyriads, Phys. Lett. **B 525**, 63 (2002).

[10] W.W.M. Allison and J.H. Cobb, Ann. Rev. Nucl. Part. Sci. **30**, 253 (1980), in particular Eq. 28 and Figs. 5&6.

[11] S. Dimopoulos, G.D. Starkman and B.W. Lynn, Mod. Phys. Lett. **A 1**, 491 (1986).

[12] L.M. Krauss, S.L. Glashow and D.N. Schramm, Nature **310**, 191 (1984).

[13] H. Bichsel, D.E. Groom, and S.E. Klein, Phys. Lett. **B 667**, 267 (2008), and references therein.

[14] W. Greiner and J. Reinhardt, *Quantum electrodynamics*, Example 3.17, Springer-Verlag (1994).

[15] C.F. Weizsäcker, Z. Phys. **88**, 612 (1934);
E.L. Williams, Phys. Rev. **45**, 729 (1934).

[16] J.A. Grifols, E. Masso, and S. Mohanty, Phys. Lett. **B 587**, 184 (2004).

[17] F. Halzen and A.D. Martin, *Quarks and Leptons*, Chapter 8.3-8.5, Wiley & Sons (1984).

[18] B.L. Henke, E.M. Gullikson, and J.C. Davis, Atomic Data and Nuclear Data Tables, **54**, 181 (1993).

[19] E. Kh. Akhmedov and V.V. Berezin, Z. Phys. **C 54**, 661 (1992);
K. Tsuji et al., Phys. Lett. **B 602**, 60 (2004).

[20] M. Deniz et al., arXiv: 0911.1597 (2009).

[21] H.T. Wong et al., J. Phys. Conf. Ser. **39**, 266 (2006);
P.A. Barbeau, J.I. Collar and O. Tench, JCAP **09**, 009 (2007).

[22] S.T. Lin et al, Phys. Rev. **D 79**, 061101(R) (2009).

[23] J.D. Lewin and P.F. Smith, Astropart. Phys. **6**, 87 (1996).

[24] K. Sigurdson et al., Phys. Rev. **D 70**, 083501 (2004).

[25] S. Dimopoulos et al., Phys. Rev. **D 41**, 2388 (1990).

[26] N.F. Bell et al., Phys. Rev. Lett. **95**, 151802 (2005);
N.F. Bell et al., Phys. Lett. **B 642**, 377 (2006).